

Energy-Based Control of a Haptic Device Using Brakes

Changhyun Cho, Jae-Bok Song, and Munsang Kim

Abstract—This paper proposes an energy-based control method of a haptic device with electric brakes. Unsmooth motion is frequently observed in a haptic system using brakes during a wall-following task. Since it is generally known that a haptic system using brakes is passive due to brake's characteristics, its energy behavior has seldom been investigated. However, force distribution at the end effector reveals that the unsmooth motion of a haptic system using brakes represents active behavior of the system in the specific direction. A force control scheme is proposed that computes the gain for smooth motion by considering the energy behavior of a system. Experiments show that smooth wall following is possible with a proposed force control scheme.

Index Terms—Brake, force approximation, indirect force control, passive force manipulability ellipsoid (FME), passivity.

I. INTRODUCTION

AS UBIQUITOUS computing environments become more popular, portable or wearable haptic devices are necessary and may create new fields such as an interactive museum tour [1]. In most cases, haptic devices need to provide enough force that can stop or at least impede the human motion, thereby requiring a large number of actuators. For portability, actuators with high power/mass ratio are desirable in haptic devices. In addition, low energy consumption of actuators is important to build smaller and lighter haptic systems.

Compared with a conventional electric motor as an actuator, a brake has an advantage of a good torque/mass ratio. Hence, use of brakes for haptic systems enables to build lighter haptic devices. Furthermore, its relatively low energy consumption makes it suitable for portable devices. Since most real or virtual environments can be modeled as passive systems, the use of brakes for haptic devices can be justified. Taking all these benefits into account, haptic devices equipped with brakes can be a good solution to portable or wearable haptic devices.

However, a brake can generate a torque only against the direction of either its motion or the external torque acting on it. Due to this limitation, a haptic device using brakes can often display a desired force only approximately. This type of force approximation, which is inevitable in the haptic devices using brakes, frequently appears during the wall-following task

Manuscript received October 19, 2005; revised May 1, 2006 and July 12, 2006. This paper was recommended by Associate Editor M. S. de Queiroz.

C. Cho and M. Kim are with the Korea Institute of Science and Technology, Center for Intelligent Robotics, Seoul 136-791, Korea (e-mail: chocho@kist.re.kr; munsang@kist.re.kr).

J.-B. Song is with the Department of Mechanical Engineering, Korea University, Seoul 136-701, Korea (e-mail: jbsong@korea.ac.kr).

Color versions of one or more of the figures in this paper are available online at <http://ieeexplore.ieee.org>.

Digital Object Identifier 10.1109/TSMCB.2006.883431

in which the user intends to move the end effector along the surface of a virtual wall. During this task, unsmooth or jagged motion (i.e., repeated contact and noncontact of the end effector with a virtual wall) is often observed [2].

Several control algorithms have been suggested to cope with this unsmooth force display. The single degree-of-freedom (SDOF) controller, in which some brakes are locked to reduce the system's DOFs, was proposed in [3]. Swanson and Book applied the optimal control technique to their velocity ratio controller, where cost functions were introduced to minimize the approximation angle and the loss of kinetic energy [4]. A small band was set up near the surface to move the end effector of the device on the surface of a virtual wall [5], and only one brake was activated in this band. From the analysis of force distribution at the end effector, brake torques can be controlled such that unsmooth force display can be eliminated during the wall-following task [6]. This control scheme, however, requires a high-precision, high-cost force/torque sensor to accurately measure the force applied by a human operator.

The energy behavior of a haptic device using brakes has seldom been investigated due to the passive nature of a brake. However, the unsmooth motion of a haptic system using brakes is similar to the unstable behavior of a haptic system using electric motors. Repeated contact and noncontact of the end effector with a virtual wall is observed in both cases. To understand the features of this unsmooth motion in a haptic system using brakes, force distribution at the end effector is investigated. This force analysis reveals that the unsmooth motion of a haptic system using brakes represents active behavior in that energy has a negative value [7]. To tackle this active behavior, the time-domain passivity control (TDPC) method proposed in [8] and [9] was extended to a haptic system using brakes in this research.

This paper is organized as follows. In Section II, the limitations of a haptic interface using brakes are investigated with passive force manipulability ellipsoid (FME) analysis. In Section III, the unsmooth wall-following motion of a brake-based haptic system is analyzed using this tool, and its energy behavior is investigated. In Section IV, an energy-based control method is proposed. In Section V, experimental results are presented, and finally, in Section VI, conclusions are drawn and future work outlined.

II. REFERENCE FORCES

In an electric brake, only the magnitude of a braking torque can be controlled, since the change in the polarity of the electromagnet does not affect its direction. A brake can generate

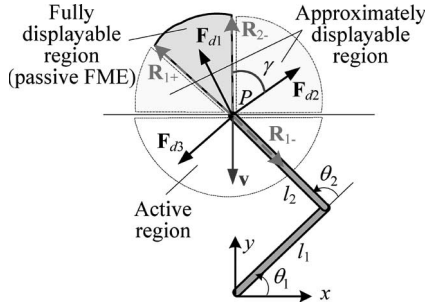


Fig. 1. Force approximation ($\theta_1 = 45^\circ$, $\theta_2 = 90^\circ$, $l_1 = l_2 = l$). Three force regions exist in task space: fully displayable region, approximately displayable region, and nondisplayable (active) region.

its braking torque τ only in the region in which $\tau \cdot \dot{\theta} \leq 0$ is satisfied, where $\dot{\theta}$ is the angular velocity of the brake shaft. Therefore, if the brake is commanded to generate a desired torque τ_d in the region in which $\tau_d \cdot \dot{\theta} > 0$, the brake control torque τ_c should be set to zero since τ_d is unachievable. Taking these observations into account, one can obtain the brake control law by adopting the Karnopp's stick-slip model [10] as follows:

Slip mode ($\dot{\theta} \neq 0$)

$$\tau_c = \begin{cases} -\text{sgn}(\dot{\theta})|\tau_d|, & \text{if } \text{sgn}(\dot{\theta}) \neq \text{sgn}(\tau_d) \\ 0, & \text{otherwise} \end{cases} \quad (1a)$$

Stick mode ($\dot{\theta} = 0$)

$$\tau_c = \begin{cases} -\text{sgn}(\tau_h)|\tau_d|, & \text{if } \text{sgn}(\tau_h) \neq \text{sgn}(\tau_d) \\ 0, & \text{otherwise} \end{cases} \quad (1b)$$

where τ_h is the external torque acting on the brake shaft (e.g., the hand torque input applied by a human operator in most haptic devices). In what follows, (1) will be referred to as the passive constraint.

A two-link manipulator is illustrated in Fig. 1, where l_i and θ_i ($i = 1, 2$) denote the length of link i and joint angle i , respectively. The end effector force \mathbf{F}_c can be obtained from the Jacobian mapping

$$\mathbf{F}_c = \mathbf{J}^{-T} \boldsymbol{\tau}_c. \quad (2)$$

For a two-link manipulator, \mathbf{J}^{-T} is given by

$$\mathbf{J}^{-T} = \frac{1}{l_1 l_2 s_2} \begin{bmatrix} l_2 c_{12} & -l_1 c_1 - l_2 c_{12} \\ l_2 s_{12} & -l_1 s_1 - l_2 s_{12} \end{bmatrix} = [\mathbf{J}_1 \mid \mathbf{J}_2] \quad (3)$$

where $c_1 = \cos(\theta_1)$, $s_1 = \sin(\theta_1)$, $c_{12} = \cos(\theta_1 + \theta_2)$, and $s_{12} = \sin(\theta_1 + \theta_2)$. Let \mathbf{R}_i be a force vector when only brake i is activated (i.e., $\tau_{c_i} \neq 0$), while the other brakes are released (i.e., no braking torques). They can be computed by

$$\mathbf{R}_{i+} = \mathbf{J}_i \quad \mathbf{R}_{i-} = -\mathbf{J}_i \quad (4)$$

where the subscript i denotes the joint number, and \mathbf{J}_i is the i th column vector of \mathbf{J}^{-T} . For example, if $\dot{\theta}_1 > 0$ (or $\dot{\theta}_1 < 0$), $\tau_{c1} < 0$ (or $\tau_{c1} > 0$) due to the passive constraint, then the force \mathbf{R}_{1-} (or \mathbf{R}_{1+}) will be activated. In what follows, \mathbf{R}_i will be referred to as the reference force which represents the force

available at the end effector by brake i . By a combination of these reference forces, the force at the end effector is generated.

Consider an example in Fig. 1 for detailed analysis. Suppose that the endpoint P is moving in the $-y$ direction (i.e., $\dot{\theta}_1 < 0$ and $\dot{\theta}_2 > 0$). The brakes can generate torques only in $\tau_{c1} > 0$ and $\tau_{c2} < 0$ because of the passive constraint and, therefore, \mathbf{R}_{1+} and \mathbf{R}_{2-} are activated. In this situation, \mathbf{R}_{1+} and \mathbf{R}_{2-} delimit the force direction in the specific region as shown in Fig. 1. This region denotes the so-called passive FME [11]. In haptic systems using motors, the joint torque space is unconstrained, so the joint actuator can generate a torque in any direction. Hence, a haptic system using motors has a complete FME which graphically illustrates the mapping between the torques in joint space and the forces in task space [12]. In haptic systems using brakes, however, the joint torque space is delimited by the passive constraint, thereby resulting in a constrained FME as explained in a tendon-driven mechanism [13].

The desired force \mathbf{F}_{d1} in this fully displayable region in Fig. 1 can be displayed accurately by the resultant force of \mathbf{R}_{1+} and \mathbf{R}_{2-} . On the other hand, the desired force \mathbf{F}_{d2} needs to be represented by the combined force of \mathbf{R}_{2-} and \mathbf{R}_{1-} . However, since the generation of \mathbf{R}_{1-} requires $\tau_{c1} < 0$ which violates the passive constraint of $\tau_{c1} \cdot \dot{\theta}_1 \leq 0$, \mathbf{F}_{d2} can be displayed only approximately by the nearest available reference force \mathbf{R}_{2-} alone. This region, therefore, is called the approximately displayable region in which the desired force can be displayed only approximately. It is convenient to define a force approximation angle γ between \mathbf{R}_{2-} and \mathbf{F}_{d2} as shown in Fig. 1, which represents the level of force approximation. That is, the most accurate force display is achieved at $\gamma = 0$, and the accuracy in force display decreases as γ increases. Finally, the desired force \mathbf{F}_{d3} in the active region cannot be displayed at all since it belongs to the active region of $\mathbf{F}_{d3} \cdot \mathbf{v} > 0$. Unlike haptic systems using motors, haptic systems using brakes possess the regions in which the desired force cannot be displayed or can be displayed only approximately. These regions can be easily found by the computation of reference forces.

III. UNSMOOTH MOTION

The wall-following task is a good example for evaluating the performance of force display, in that the end effector moves on the surface of a virtual wall. It is difficult, however, to achieve smooth and accurate movement along the surface with a haptic device using brakes. Its actual movement usually becomes somewhat unsmooth (i.e., contact and noncontact of the end effector with a virtual wall).

A. Pullback Capability

Consider forces acting on the end effector. They are illustrated in Fig. 2 for different penetration depths which give different values of the desired force \mathbf{F}_d . The vectors \mathbf{n} and \mathbf{t} are the unit vectors normal and tangent to the virtual wall, respectively. The wall is assumed to possess neither damping nor friction on its surface. Since the desired force \mathbf{F}_d to display the wall should be normal to the wall surface, this force can

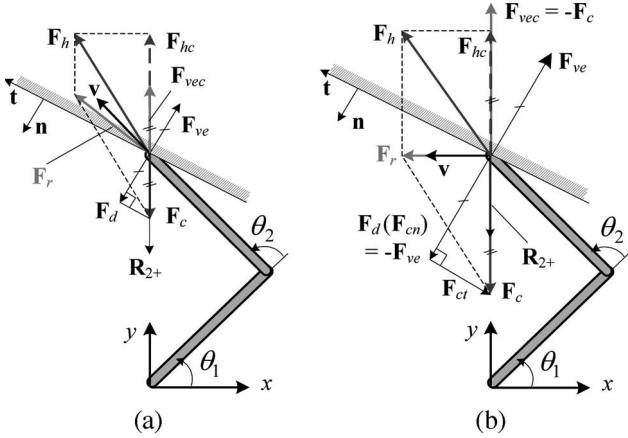


Fig. 2. Forces acting on the end effector for different penetration depths. (a) Small penetration depth: $\|\mathbf{F}_{hc}\| > \|\mathbf{F}_c\|$. (b) Large penetration depth: $\|\mathbf{F}_{hc}\| = \|\mathbf{F}_c\|$.

be displayed only approximately by the nearest reference force \mathbf{R}_{2+} . The control force \mathbf{F}_c generated by brake 2 and the hand force \mathbf{F}_h given by the user act on the end effector, thus generating \mathbf{F}_r , the resultant force of \mathbf{F}_c and \mathbf{F}_h .

At the initial contact with the virtual wall, the penetration depth is small, so $\|\mathbf{F}_{hc}\| > \|\mathbf{F}_c\|$ [i.e., case (a) in Fig. 2], where \mathbf{F}_{hc} represents the component of \mathbf{F}_h in the direction of \mathbf{F}_c . Note that for small penetration depth, the control force \mathbf{F}_c whose normal component \mathbf{F}_{cn} corresponds to \mathbf{F}_d also becomes small. Hence, the slip mode given by (1a) occurs at brake 2, and \mathbf{F}_r has a normal component directed into the wall, thus resulting in increasing penetration. As penetration continues, the control force grows to reflect an increase in wall deflection until $\|\mathbf{F}_c\| = \|\mathbf{F}_{hc}\|$ [i.e., case (b)] is reached. In this case, the normal component of the resultant force \mathbf{F}_r is directed out of the wall, thereby moving the end effector off the wall surface. It has been considered only possible in haptic devices using motors, since this pullback motion is executed by electric motors generating a force proportional to wall deformation. However, the force analysis shows that force approximation caused by the limited capability of brakes can make the pullback motion available even for haptic devices using brakes as well.

B. Energy Behavior

Now, consider the energy behavior of a haptic device using brakes. At first, the concept of passivity is briefly introduced. Fig. 3 illustrates a virtual spring and its one-port network. This network element is defined to be passive, if and only if

$$E(k) = \sum_{n=0}^k f_{ve}(n-1)v(n)T + E(0) \geq 0, \quad \forall kT \geq 0 \quad (5)$$

where $E(0)$ is the initially stored energy at $t = kT = 0$ [8], [9]. T is the sampling period, and $v(k)$ is assumed to be $\{x(k) - (x(k-1))\}/T$, where $x(k)$ denotes the position of the end effector of a haptic device at time k . Note that for a discrete-time system the effect of $f_{ve}(k-1)$ on the energy is measured at time kT , since $f_{ve}(k-1)$ is computed at time

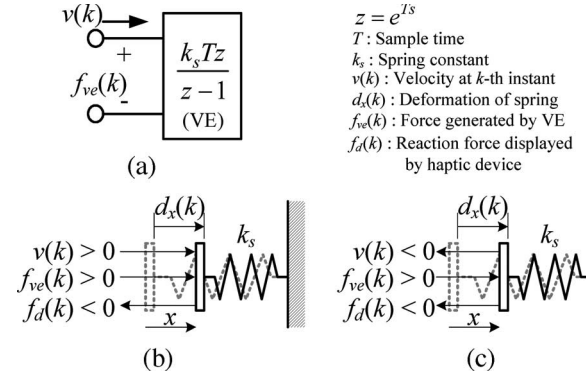


Fig. 3. One-port network. (a) Virtual spring. (b) Compression. (c) Restoration.

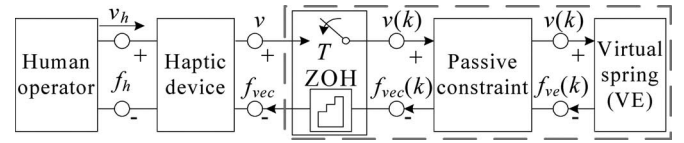


Fig. 4. SDOF haptic interface using a brake.

$k-1$ and applied during $(k-1)T \leq t < kT$. Hence, the power input is obtained by $f_{ve}(k-1) \cdot v(k)$. Further detail on the discretization technique can be referred to [14].

Equation (5) implies that a passive network cannot generate more energy than it has stored at $t = 0$ and received by the network. Note that the velocity is an input to the network, which generates the output force f_{ve} and vice versa. Therefore, the energy increases when the spring is deformed in the direction of the applied external force as shown in Fig. 3(b), i.e., the input power $f_{ve}(k-1) \cdot v(k) > 0$, whereas the energy decreases during restoration as shown in Fig. 3(c), i.e., $f_{ve}(k-1) \cdot v(k) < 0$. Note that a haptic device should generate $f_d(k) (= -f_{ve}(k))$ to retard or stop further deformation of a virtual spring, so the negative sign is given at f_{ve} as shown in Fig. 3(a).

An SDOF haptic interface using a brake is illustrated in Fig. 4. A human operator is assumed to move the end effector at a velocity of v_h and the subsequent velocities are assumed to be equal to v_h . The force $f_{ve}(k)$ is the force given by the physical laws in the virtual environment (VE) at k th time instant, and $f_{vec}(k)$ is the control force modified from $f_{ve}(k)$ by the brake control scheme (i.e., the passive constraint). Note that $f_d(k)$ and $f_c(k)$ in the passive constraint can be computed by $f_d(k) = -f_{ve}(k)$ and $f_c(k) = -f_{vec}(k)$ as shown in Fig. 2. It is well known that a network interface is unconditionally stable, if all ports in a network interface are passive [7]. If the passive constraint is omitted in the interface shown in Fig. 4, an interface using a motor is obtained and is never be unconditionally stable, because it has the active elements such as time delay caused by low update rate of VE and the sample and hold [14]–[16].

However, an SDOF haptic interface using a brake is unconditionally stable. The human operator is passive in the range of frequencies of interest in haptics [17]. A haptic device is an electromechanical system which is assumed to be passive. Thus, energy behavior of the box area in Fig. 4 are should be investigated to verify unconditional stability. Consider a

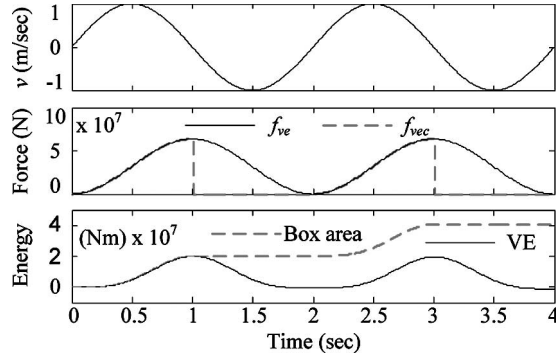


Fig. 5. Simulation results of the box area in Fig. 4 ($k_s = 1.0e^7$ N/m, $T = 0.01$ s).

virtual spring shown in Fig. 3. From the passive constraint, (1), $f_{vec}(k)$ is identical to $f_{ve}(k)$ during compression (i.e., $f_{ve}(k-1)v(k) \geq 0$). During restoration (i.e., $f_{ve}(k-1)v(k) < 0$), $f_{vec}(k)$ is set to zero by the passive constraint. Considering $f_{vec}(t) = f_{vec}(kT)$ for $kT \leq t < (k+1)T$, the input power of the box area in Fig. 4 is computed during compression, i.e., $f_{ve}(k-1)v(k) \geq 0$, $f_{vec}(t) = f_{vec}(kT) = f_{ve}(kT)$

$$P(t) = f_{vec}(t)v(t) \geq 0 \text{ where } v(t) \geq 0 \text{ and } f_{ve}(kT) > 0. \quad (6a)$$

During restoration, i.e., $f_{ve}(k-1)v(k) < 0$, $f_{vec}(t) = f_{vec}(kT) = 0$

$$P(t) = f_{vec}(t)v(t) = 0. \quad (6b)$$

Since the box area has only positive power for all cases from (6), the energy of the box area remains positive all the time. For verification, simulation of the box area is conducted, and its results are shown in Fig. 5. A virtual spring is modeled as $k_s T z / (z - 1)$, where $z = e^{Ts}$ and k_s and T denotes a spring constant and sample interval, respectively. The velocity, v , is given as an input for simulation. Note that v cannot have negative values for real haptic interface in Fig. 4, since a pullback capability is not possible by a brake at all for an SDOF haptic interface. As mentioned before, f_{vec} is identical to f_{ve} during compression. In Fig. 5, the energy of the box area remains positive all the time and has a constant value during restoration, whereas that of VE goes negative. That is, the box area in Fig. 4 is passive due to the passive constraint.

Therefore, an SDOF haptic interface using a brake is unconditionally stable, since all elements are passive or behaves like a passive element. The energy behavior of the box area in Fig. 5 is termed as the ideal display in this paper. Note that (6b) never happen in a haptic interface using a motor, so energy is generated at the box area due to the active elements as generally known. It is also noted that the transparency cannot be achieved by a haptic interface using a brake due to the nonlinear behavior of the passive constraint, since $f_{ve}(k) \neq f_{vec}(k)$ for some k .

For a multidegree-of-freedom (MDOF) interface using brakes, however, unconditionally stability cannot be achieved. An MDOF case is shown in Fig. 6 and variables are illustrated in bold characters to represent a vector form. The force approximation is employed in Fig. 6 instead of the passive constraint in Fig. 4. Consider power input of the box area in Fig. 6. The

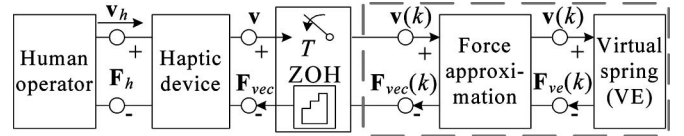


Fig. 6. MDOF haptic interface using brakes.

input power, $\mathbf{F}_{vec}(k-1) \cdot \mathbf{v}(k)$, in Fig. 6 always happens to be $\mathbf{F}_{vec}(k-1) \cdot \mathbf{v}(k) \geq 0$ due to passive nature of the force approximation. Without loss of generality, $\mathbf{F}_{vec}(k-1) \cdot \mathbf{v}(k)$ can be represented by $\mathbf{F}_{vec_n}(k-1) \cdot \mathbf{v}_n(k) + \mathbf{F}_{vec_t}(k-1) \cdot \mathbf{v}_t(k)$, where \mathbf{x}_n and \mathbf{x}_t denote the vectors in the direction parallel and perpendicular to $\mathbf{F}_{ve}(k)$, respectively. For an MDOF case the velocity and force projected onto $\mathbf{F}_{ve}(k)$ should be considered as in [8]. It is desirable that any force compensation such as additional damping, which would be required to stabilize a haptic interface, should be applied in the direction of the desired force. Damping in the perpendicular direction retards free motion, whereas that in the parallel direction is used to stabilize a haptic system.

From Fig. 2(b), an MDOF haptic system using brakes obtains pullback capability, i.e., restoration in Fig. 3, due to force approximation and $\mathbf{F}_{vec_n}(k)$ is identical to $\mathbf{F}_{ve}(k)$ during force approximation, $\mathbf{F}_d = \mathbf{F}_{cn}$ in Fig. 2. Thus, $\mathbf{F}_{vec_n}(k-1) \cdot \mathbf{v}_n(k) < 0$ during restoration and $\mathbf{F}_{vec_n}(k-1) \cdot \mathbf{v}_n(k) \geq 0$ during compression. That is, the box area in Fig. 6 can generate positive and negative power in the parallel direction to \mathbf{F}_{ve} . Thus, the element of the force approximation in the parallel direction to \mathbf{F}_{ve} can be removed and the interface in Fig. 6 in the parallel direction to \mathbf{F}_{ve} becomes identical to an interface using motors, which is never be unconditionally stable due to the active elements such as time delay caused by low update rate of VE and the sample and hold. Therefore, unconditional stability in the parallel direction to \mathbf{F}_{ve} cannot be achieved for an MDOF haptic interface using brakes, if force approximation is made. In this situation, if energy generated by the active elements is greater than the total energy of passive elements (e.g., human operator, haptic device), unsmooth motion is activated in the direction parallel to \mathbf{F}_{ve} .

If no force approximation is made, no pullback capability is obtained (i.e., $\mathbf{F}_{rn} = 0$) and \mathbf{v}_n becomes zero, thereby resulting in $\mathbf{F}_{vec_n} \cdot \mathbf{v}_n = 0$ as in the SDOF case in Fig. 4. However, this situation rarely happens during wall-following task. Note that \mathbf{F}_{ct} always has a sign opposite to human operator's intention (i.e., \mathbf{v}_t or \mathbf{F}_{ht}) as shown in Fig. 2. Therefore, \mathbf{F}_{ct} ($= -\mathbf{F}_{vec_t}$) plays no role in achieving smooth motion and just retards free motion of the end effector along the wall surface.

IV. INDIRECT FORCE CONTROL METHOD

It was observed in Section III that the pullback force was activated because of the force approximation in a haptic device using brakes and the unsmooth motion was caused by this pullback force and any active elements such as time delay. If one can make velocity in the normal direction remain at zero value after initial contact with a virtual wall, no repeated contact and noncontact motion will be activated, thereby leading to smooth wall following. In this situation the input power $\mathbf{F}_{cn} \cdot \mathbf{v}_n$

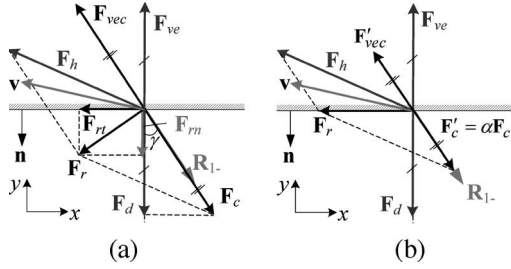


Fig. 7. Forces acting on the end effector. Force approximation can provide active resultant force, which enables the pullback motion.

becomes zero because of $v_n = 0$, and the energy in the direction parallel to a desired force remains at the positive region for all time. Hence, a smooth wall following can be achieved regardless of time delay by making the normal component of the resultant force \mathbf{F}_r in Fig. 2(b) vanish. This underlying idea of the direct force control scheme is proposed in this research.

Fig. 7 illustrates various forces involved in representing a virtual wall. Proper brake control can be found by observing the relations of these forces. If the desired force \mathbf{F}_d is to be displayed approximately by the reference force \mathbf{R}_{1-} , for example, then the control force \mathbf{F}_c is generated in the direction of \mathbf{R}_{1-} with an approximation angle γ between \mathbf{F}_d and \mathbf{F}_c . The resultant \mathbf{F}_r of all the forces acting on the end effector becomes

$$\mathbf{F}_r = \mathbf{F}_{rn} + \mathbf{F}_{rt} = \mathbf{F}_h + \mathbf{F}_c \quad (7)$$

where \mathbf{F}_{rn} and \mathbf{F}_{rt} are the normal and tangential components of \mathbf{F}_r . In Fig. 7(a), \mathbf{F}_{rn} is directed out of the wall, thus moving the end effector off the wall surface.

Because unsmooth wall following is caused by repeated contact and noncontact of the end effector with the wall, the proposed brake control attempts to make the normal component \mathbf{F}_{rn} go to zero by adjusting the brake torques (e.g., reducing brake torques) as shown in Fig. 7(b). Then, the end effector becomes subject to only the tangential force along the surface; therefore, it can follow the wall smoothly without leaving the wall surface. A new control force \mathbf{F}'_c is given by

$$\mathbf{F}'_c = \alpha \mathbf{F}_c \quad (8)$$

where α is the scale factor. Substitution of (8) into (7) yields

$$\mathbf{F}_h + \mathbf{F}'_c = \mathbf{F}_h + \alpha \mathbf{F}_c. \quad (9)$$

Since \mathbf{F}_r is normal to \mathbf{F}_d with the new control force \mathbf{F}'_c , $(\mathbf{F}_h + \alpha \mathbf{F}_c) \cdot \mathbf{F}_d = 0$, and the following relation is obtained:

$$\alpha = -(\mathbf{F}_h \cdot \mathbf{F}_d) / (\mathbf{F}_c \cdot \mathbf{F}_d). \quad (10)$$

Although α can be computed accurately from (10), this computation requires the precise measurement of \mathbf{F}_h , which is usually carried out by a high-cost force/torque sensor. Therefore, an energy-based approach is proposed in this research to compute the scale factor α without resorting to the precise measurement of \mathbf{F}_h . Since α is computed indirectly by the energy-based approach, the proposed control scheme will be referred to as the indirect force control.

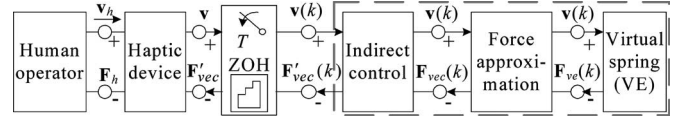


Fig. 8. Network representation of haptic interface using brakes with the indirect control.

The TDPC proposed by Hannaford and Ryu has simple implementation and robustness since it does not need the dynamic model of a haptic system which is nonlinear in most cases [8], [9]. Taking these advantages into account, the framework of TDPC (i.e., numerical computation of energy in the time domain) is applied in this research.

On the basis of Fig. 6, a haptic interface using brakes with the indirect control is illustrated in Fig. 8. \mathbf{F}'_{vec} is the force computed by the indirect force control scheme. Since the unsmooth motion of a haptic device using brakes is caused by both time delay (due to the low update rate of VE) and force approximation, computation of the energy should take these active elements into account. Referring to (5), a discrete-time form of the stored energy $E(n)$ of the dashed area in Fig. 8 can be represented by

$$E(n) = \sum_{k=1}^n \mathbf{F}'_{vec}(k-1) \cdot \mathbf{v}(k)T + E(0) \quad (11)$$

where T is the sampling period and $\mathbf{v}(k)$ is assumed to be $\{\mathbf{x}(k) - \mathbf{x}(k-1)\}/T$, where $\mathbf{x}(k)$ denotes the position of the end effector of a haptic device at time k .

The energy computed by (11) always has a positive value, since $\mathbf{F}_{vec}(k-1) \cdot \mathbf{v}(k) \geq 0$ for all time due to passive nature of a brake. As mentioned in Section III, however, the energy in the direction parallel to \mathbf{F}_{ve} can have a negative value due to active elements such as time delay, since $\mathbf{F}_{vec_n}(k-1) \cdot \mathbf{v}_n(k)$ can have a negative value due to force approximation, where \mathbf{x}_n denotes the vectors in the direction parallel to \mathbf{F}_{ve} . Hence, the energy in the direction parallel to \mathbf{F}_{ve} should be observed.

Let v_n and f'_{vec_n} be components of \mathbf{v} and \mathbf{F}'_{vec} in the direction parallel to \mathbf{F}_{ve} . From (10), the energy in the direction parallel to \mathbf{F}_{ve} can be computed by

$$E_n(n) = \sum_{k=1}^n f'_{vec_n}(k-1)v_n(k)T + E_n(0). \quad (12)$$

From (8), f'_{vec_n} can be computed by

$$f'_{vec_n}(k) = \alpha(k)f_{vec_n}(k). \quad (13)$$

Substitution of (13) into (12) yields

$$E_n(n) = \sum_{k=1}^n \alpha(k-1)f_{vec_n}(k-1)v_n(k)T + E_n(0). \quad (14)$$

The control objective is to regulate braking torques to imitate the ideal force display in that energy of a haptic system using a brake has a positive constant value during contact as shown in Fig. 5. Energy plots for both ideal and actual situations

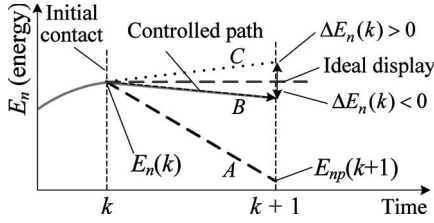


Fig. 9. Energy plots as a function of time, showing the concept of energy-based control.

are illustrated in Fig. 9. In the ideal force display, the energy does not change after the initial contact with the wall (i.e., $f'_{\text{vec}_n}(k-1)v_n(k) = 0$) because $v_n(k) = 0$ owing to no pull-back capability. However, if the pullback motion occurs due to force approximation, then $f'_{\text{vec}_n}(k-1)v_n(k) < 0$ and the energy may steeply decrease as in path A. If the situation continues, the unsmooth motion is likely to occur because the energy becomes negative. In this case, path A should be shifted toward the ideal path by properly adjusting $\alpha(k)$.

To execute this control strategy, consider the change of energy for one sampling period for the dashed area in Fig. 9. Let $\Delta E_n(k) = E_{np}(k+1) - E_n(k)$, where $E_{np}(k+1)$ is the energy of time $k+1$ predicted at time k and $E_n(k)$ is the actual energy at k . $\Delta E_n(k)$ can be computed by

$$\Delta E_n(k) = \alpha(k) f'_{\text{vec}_n}(k) v_n(k) T. \quad (15)$$

$\Delta E_n(k) > 0$ (or $\Delta E_n(k) < 0$) denotes an increase (or decrease) in energy. For the ideal display, $\Delta E_n(k) = 0$ as shown in Figs. 5 and 9, because $v_n(k) = 0$ or $f'_{\text{vec}_n}(k) = 0$ owing to no pullback motion.

It is seen from (15) that $\alpha(k)$ can be determined by selecting a desired $\Delta E_n(k)$ so that the haptic system using brakes exhibits the ideal energy behavior. Let ΔE_{nd} be the desired change of energy. Setting ΔE_{nd} to zero to imitate this ideal display leads to $\alpha(k) = 0$ (because usually $v_n(k) f'_{cn}(k) \neq 0$), thus resulting in fully releasing of all brakes ($f'_{\text{vec}_n}(k) = \alpha(k) f'_{\text{vec}_n}(k) = 0$). The total power of the sample and hold and the dashed area in Fig. 8 will not have negative value due to the zero input $f'_{\text{vec}_n}(k) = 0$ after initial contact as in the SDOF haptic interface in Fig. 4, thereby result in positive energy. Since the human operator and haptic device are passive, unconditional stability is guaranteed in this situation.

For real implementation, however, it is desirable to have ΔE_{nd} be set to a very small nonzero value in order to avoid fully releasing of all brakes. Since path C corresponding to the positive ΔE_{nd} increases penetration of the end effector, ΔE_{nd} should have a negative sign as indicated in path B to avoid further penetration during force control. Since ΔE_{nd} will be set to a very small negative value, very small energy decreases occur during the sample interval. Considering stored energy after initial contact and absorbed energy by the other passive elements (the human operator and haptic device), a very small negative value of ΔE_{nd} is acceptable for real implementation.

It is reasonable that $\alpha(k)$ is computed from (15) only when the end effector is inside the wall but moves outwardly (i.e., during the pullback motion), because the outward motion may cause unstable behavior as explained in the previous sec-

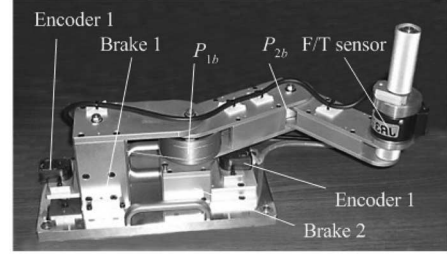
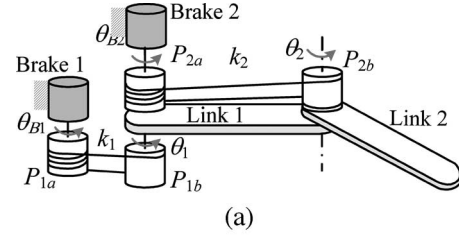


Fig. 10. Coupled tendon-drive mechanism. (a) Schematic. (b) Photo.

tion. When the end effector continues to move into the wall, brakes are firmly activated to retard its penetration. Note that $\alpha(k) > 1$ means that the brake is commanded to generate a higher torque than necessary to provide the desired force, which is unreasonable. From these observations, $\alpha(k)$ can be computed by

$$\alpha(k) = \begin{cases} \Delta E_{nd} / \{v_n(k) f'_{\text{vec}_n}(k) T\}, & \text{if } v_n(k) f'_{\text{vec}_n}(k) T < \Delta E_{nd} \\ 1, & \text{otherwise} \end{cases} \quad (16)$$

where $\Delta E_{nd} < 0$. Since $f'_{\text{vec}_n}(k) v_n(k) T < \Delta E_{nd} < 0$, $0 < \alpha(k) < 1$. Force is adjusted by nonlinear control action, so transparency cannot be achieved as that in Fig. 4. Implementation of the indirect force control is summarized as follows.

- 1) Compute $f'_{\text{vec}_n}(k)$ according to the passive constraint.
- 2) Obtain $\alpha(k)$ from (16).
- 3) Find the modified control force $\mathbf{F}'_{\text{vec}}(k) = \alpha(k) q \mathbf{F}_{\text{vec}}(k)$.
- 4) Generate the brake torque $\tau'_{\text{vec}}(k)$ to deliver $\mathbf{F}'_{\text{vec}}(k)$ using the Jacobian relation.

Note that the desired change of energy, ΔE_{nd} , is a crucial parameter to the performance of a haptic system, since it is used to classify energy behavior as active or passive and to activate a control action.

V. EXPERIMENTS

In the previous section, the indirect force control method was introduced. This method will be verified through experiments using a two-link mechanism equipped with two electric brakes.

The two-link haptic device equipped with two electric brakes shown in Fig. 10 was constructed for experiments. The angles θ_i and θ_{B_i} represent the joint angle and the rotating angle of the brake, respectively, and k_i is the reduction ratio of the tendon-drive system. The design parameters are $k_1 = 0.2$, $k_2 = 0.4$, and $l_1 = l_2 = 0.15$ m. Brake 1 (or 2), which provides a braking torque to link 1 (or 2), is mounted at the base and conveys

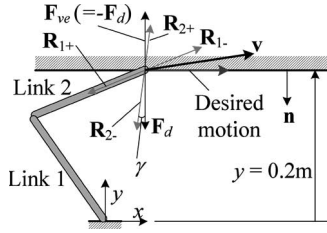


Fig. 11. Location of virtual wall and experimental conditions.

the torque through pulleys $P_{1a} - P_{1b}$ (or $P_{2a} - P_{2b}$). The joint angle θ_2 is described by

$$\theta_2 = k_2\theta_{B2} - k_2\theta_1. \quad (17)$$

Note that θ_2 is a function of θ_1 as well as θ_{B2} . That is, the coupled motion in the wire transmission is observed in θ_2 . The Jacobian is obtained by

$$\mathbf{J} = \begin{bmatrix} -l_1 s_1 - l_2(1 - k_2)s_c & -k_2 l_2 s_c \\ l_1 c_1 + l_2(1 - k_2)c_c & k_2 l_2 c_c \end{bmatrix} \quad (18)$$

where $c_1 = \cos(\theta_1)$, $s_1 = \sin(\theta_1)$, $c_c = \cos((1 - k_2)\theta_1 + k_2\theta_{B2})$, $s_c = \sin((1 - k_2)\theta_1 + k_2\theta_{B2})$, and l_i represents the link length.

Since the sign of the hand torque given by the user is required to compute the passive constraint 1(b), the force/torque sensor is mounted at the handle of the end effector. Note that not the accurate readings of the hand force/torque but only the sign of the hand torque is needed to implement the indirect force control. Rotational motion of each brake is sensed by the optical encoder mounted on the brake axis.

In the experiments, brake control was executed at a rate of 1 kHz. The brake generated a braking torque in proportion to the input current. Note that precise control of a brake, which has the nonlinear characteristics, is not easy and requires the measurement of the hand torque input [18]. In general, precise control of a brake can improve the performance of a haptic system, but it is not strictly required for the energy-based control method, since the brake torque is controlled by the energy behavior of VE or a haptic device, which is the result of dynamic behavior of both brakes and a mechanism. The plane virtual wall was implemented and its surface was located at $y = 0.2$ m as shown in Fig. 11. The virtual wall was modeled as a spring whose spring constant was 10^7 N/m, but it was assumed to possess neither damping nor friction on the surface. A hand force input was provided to move the handle mounted at the end effector in the $+x$ direction while it maintained contact with the virtual wall. The ΔE_{nd} was experimentally determined and was set to -0.001 N · m.

In this situation, \mathbf{R}_{2-} was used to display the virtual wall as a shown in Fig. 11, since \mathbf{F}_d exists at the outside of the region delimited by \mathbf{R}_{1+} and \mathbf{R}_{2-} ($\theta_1 < 0, \theta_{B2} > 0$). Thus, only brake 2 was activated with brake 1 fully released during force display, so the control force $\mathbf{F}_c (= -\mathbf{F}_{vec})$ had the same direction as \mathbf{R}_{2-} . The approximation angle γ , an angle between the desired and the control force as shown in Fig. 1, increased as the end effector moved in the $+x$ direction. The minimum and

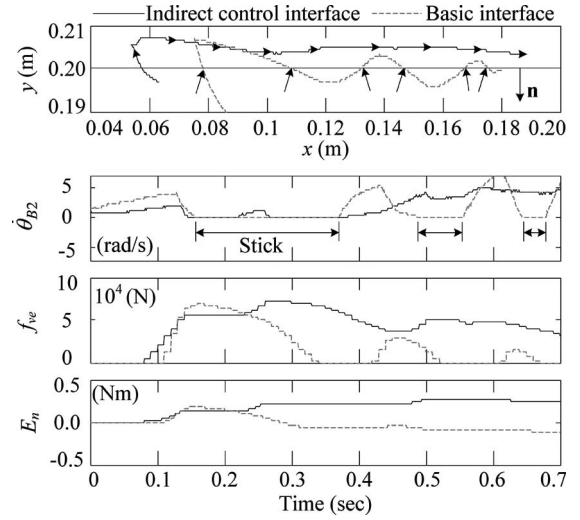


Fig. 12. Experimental results on a plane wall at the virtual wall update rate of 100 Hz.

maximum approximation angles were 3° around $x = 0.06$ m and 37° around $x = 0.18$ m, respectively.

Suppose that the end effector moves in the $-x$ direction at the given configuration as shown in Fig. 11. In this case, the passive FME delimited by \mathbf{R}_{1-} and \mathbf{R}_{2+} is activated, but \mathbf{F}_d cannot be displayed with \mathbf{R}_{1-} and \mathbf{R}_{2+} . Thus, all brakes are fully released. As penetration increases, therefore, the configuration of the two-link mechanism changes and the directions of the reference forces also vary. The desired force soon belongs to the fully displayable region delimited by \mathbf{R}_{1-} and \mathbf{R}_{2-} , so no force approximation is made, thereby resulting in no pullback motion. The proposed control scheme therefore will not be applied to this case.

The experimental results in Figs. 12 and 13 were obtained at the virtual wall update rate of 100 Hz. We observed that the excessive penetration into the wall occurred initially around $x = 0.06$ m, although the wall was stiff enough to prevent such penetration (i.e., 10^7 N/m). This penetration was attributed mainly to time delay caused by the slow update of the virtual wall and the slow response time of the brakes. Hence, a slower velocity of the end effector into the wall and/or use of brakes with faster response time would reduce the penetration depth. Note for experiments that the basic interface represents the MDOF haptic interface in Fig. 6 and the indirect control interface denotes the interface implementing the indirect force control shown in Fig. 8, respectively.

Smooth paths of the end effector were observed after the first contact for the indirect control interface shown in Fig. 12. The penetration depth also remained at a relatively constant value, whereas unsmooth motion (i.e., contact and noncontact) was repeated on the basic interface (i.e., arrow markers in Fig. 12). The basic interface sometimes exhibits active behavior (i.e., energy < 0 as shown in the energy plot in Fig. 12), whereas the indirect control interface shows passive behavior for all time from the viewpoint of passivity. The energy moderately increased with time during the indirect force control in Fig. 12. We observed from the θ_{B2} plot that the duration of the stick mode was much shorter for the indirect control interface than

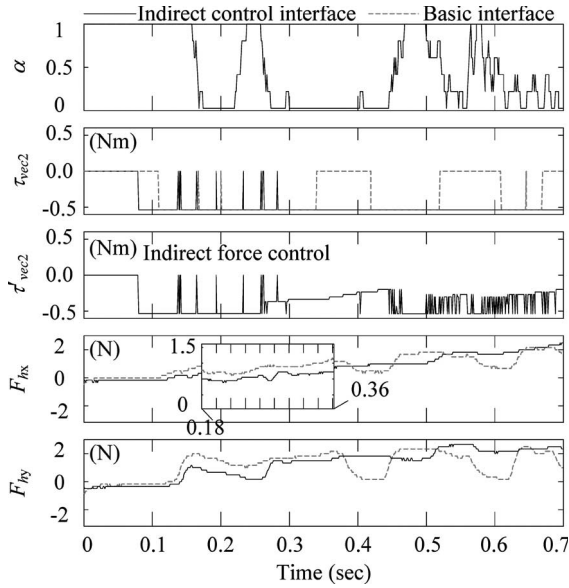


Fig. 13. Control output and hand force input of experiments in Fig. 12.

for the basic interface, thus indicating that brake 2 was not completely locked during the indirect force control.

The indirect force control scheme allows the brakes to slip when pullback motion is generated. This can be reconfirmed by the plots of τ_{vec2} and τ'_{vec2} in Fig. 13. Note that τ_{vec2} represents a torque command of brake 2 computed by force approximation using the Jacobian relation and τ'_{vec2} denotes a torque command of brake 2 computed by indirect force control. Without force control (i.e., $\tau'_{vec2} = \tau_{vec2}$), τ_{vec2} was set to the maximum value of 0.565 N·m during the wall contact, so brake 2 was fully locked. However, τ'_{vec2} computed by the indirect force control method was not always saturated at the maximum value and showed the slip mode in brake 2. In general, saturation in reference torque should be implemented due to torque limit of brakes. The oscillation in the τ'_{vec2} is mainly caused by the torque saturation. Also, noise in velocity may generate the oscillation, since the gain, α , computed by the indirect control method is determined by the sign of input power which is computed by velocity and force. Consider the hand force input by the human operator. F_{hx} and F_{hy} denote components of the hand force input in the x and y directions. F_{hy} in Fig. 13 changed gradually during force control without sudden variations that frequently occurred at the basic interface. The gain α was nearly zero because of the small hand force ($F_{hy} < 2.5$ N) compared to the large desired force (5×10^4 N).

It is also noted that the tangential component of a hand force F_{hx} increases as the approximation angle γ increases. It means that a human operator feels a stronger force, which retards the motion along the surface as γ increases. This can be easily understood by investigating the forces acting on the end effector as shown in Fig. 7. That is, the undesired force, $|\alpha \mathbf{F}_c| \sin \gamma$, due to force approximation increases with γ , but this value is less than the force $|\mathbf{F}_c| \sin \gamma$ for no control because $0 < \alpha \leq 1$. As a result, a human operator feels less retarding force along the surface with the indirect force control as shown in the enlarged plot of F_{hx} in Fig. 13.

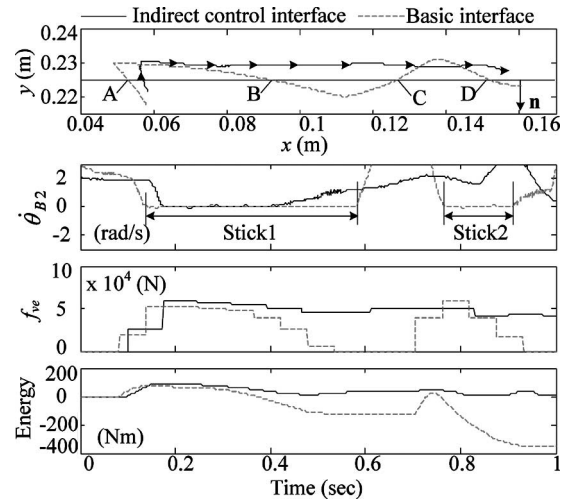


Fig. 14. Experimental results on a plane wall at the virtual wall update rate of 20 Hz.

Experimental results for update rate of 20 Hz are presented in Fig. 14. The features observed in Fig. 13 are similarly observed in Fig. 14. As the update rate of VE decreases, the basic interface rapidly became active, i.e., the energy of the basic interface rapidly goes to the negative region, whereas that of the indirect control interface remains in the positive region by the control action.

VI. CONCLUSION

In this research, the energy-based force control method for a haptic device using brakes was proposed to overcome its unsmooth behavior during a wall-following task. It was proven that pullback capability is obtained by the force approximation, which is inevitable to achieve force display for an MDOF haptic device using brakes. Unconditional stability of an SDOF haptic interface using a brake was verified. It was shown that the MDOF interface became identical to a haptic interface using motors in the desired force direction, if force approximation is made, i.e., the pullback capability is obtained. An energy-based control was proposed in that force of the MDOF interface is regulated to imitate the energy behavior of the SDOF interface. From experiments, the following conclusions can be drawn.

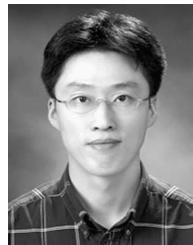
- 1) A haptic device using brakes can show good performance when it involves either time delay alone or force approximation alone. A haptic device using brakes involving both time delay and force approximation may exhibit poor performance.
- 2) The indirect force control scheme can improve the performance of force display regardless of time delay without any precise measurement of the hand force input.
- 3) An undesired force due to force approximation retards the motion of the end effector along the surface. This retarding force increases as the approximation angle increases, but can be reduced by the indirect force control.
- 4) Unsmooth motion of a haptic device using brakes can be explained by investigating the energy plot under passivity criteria. As the unsmooth motion continues, the

energy becomes more negative, thus resulting in the active behavior.

Virtual sculpting would be a good example for a haptic device using brakes, since plastic deformation should be implemented and is purely passive. Also, it requires tool path guidance, and performance of path guidance can be greatly improved by the proposed energy-based control scheme. The electric brakes with faster response time are needed to obtain better force display performance for the proposed indirect force control scheme. Furthermore, a method needs to be developed for estimating the absorbed energy of the passive elements such as a human operator and a haptic device in order to prevent the overconservative action of the controller.

REFERENCES

- [1] C. S. Hwang, D. S. Ryu, and C. H. Cho, "Development of a wearable and lightweight haptic device for man and environment interface in the intelligent environment," *J. KSPE*, vol. 21, no. 11, pp. 12–16, Nov. 2004. (in Korean).
- [2] J. E. Colgate, M. A. Peshkin, and W. Wannasupphrasit, "Nonholonomic haptic display," in *Proc. IEEE Int. Conf. Robot. and Autom.*, Apr. 1996, vol. 1, pp. 539–544.
- [3] D. K. Swanson and W. J. Book, "Obstacle avoidance methods for a passive haptic display," in *Proc. IEEE Int. Conf. Adv. Intell. Mechatronics*, Jul. 2001, vol. 2, pp. 1187–1192.
- [4] —, "Path-following control for dissipative passive haptic displays," in *Proc. 11th Symp. Haptics*, Mar. 2003, pp. 101–108.
- [5] M. Sakaguchi, J. Furusho, and N. Takesue, "Passive force display using ER brakes and its control experiments," in *Proc. Virtual Reality*, Mar. 2001, pp. 7–12.
- [6] C. H. Cho, M. S. Kim, and J. B. Song, "Direct control of a passive haptic device based on passive force manipulability ellipsoid analysis," *Int. J. Control. Autom. Syst.*, vol. 2, no. 2, pp. 238–246, Jun. 2004.
- [7] S. S. Haykin, *Active Network Theory*. Reading, MA: Addison-Wesley, 1970, ch. 3, pp. 104–119.
- [8] J. H. Ryu, Y. S. Kim, and B. Hannaford, "Sampled- and continuous-time passivity and stability of virtual environments," *IEEE Trans. Robot.*, vol. 20, no. 4, pp. 772–776, Aug. 2004.
- [9] C. Preusche, G. Hirzinger, J. H. Ryu, and B. Hannaford, "Time domain passivity control for 6 degrees of freedom haptic displays," in *Proc. IEEE/RJS Int. Conf. Intell. Robot. and Syst.*, Oct. 2003, vol. 3, pp. 2944–2949.
- [10] D. Karnopp, "Computer simulation of stick-slip friction in mechanical dynamic system," *Trans. ASME, J. Dyn. Syst. Meas. Control*, vol. 107, no. 1, pp. 100–103, Mar. 1985.
- [11] C. H. Cho, J. B. Song, and M. S. Kim, "Design and control of a planar haptic device with passive actuators based on passive force manipulability ellipsoid (FME) analysis," *J. Robot. Syst.*, vol. 22, no. 9, pp. 475–486, Jul. 2005.
- [12] T. Yoshikawa, *Foundations of Robotics: Analysis and Control*. Cambridge, MA: MIT Press, 1990, ch. 4, pp. 127–154.
- [13] C. Mechiorri and G. Vassura, "A performance index for under-actuated, multi-wire haptic interface," in *Proc. IEEE Int. Conf. Robot. and Autom.*, Apr. 1998, pp. 1026–1031.
- [14] S. Stramigioli, C. Secchi, A. J. van der Schaft, and C. Fantuzzi, "A novel theory for sample data system passivity," in *Proc. IEEE/RJS Int. Conf. Intell. Robot. and Syst.*, vol. 2, Sep. 2002, pp. 1936–1941.
- [15] B. Gillespie and M. Cutkosky, "Stable user-specific rendering of the virtual wall," in *Proc. ASME Int. Mech. Eng. Conf. and Expo.*, 1996, vol. 58, pp. 397–406.
- [16] R. J. Adams and B. Hannaford, "Stable haptic interaction with virtual environments," *IEEE Trans. Robot. Autom.*, vol. 15, no. 3, pp. 465–474, Jun. 1999.
- [17] N. Hogan, "Controlling impedance at the man/machine interface," in *Proc. IEEE Int. Conf. Robot. and Autom.*, May 1989, pp. 1626–1631.
- [18] D. K. Swanson, E. Romagna, W. J. Book, and A. Barraco, "Influence of actuator dynamics on passive haptic interface performance," in *Proc. IEEE/ASME Int. Conf. Adv. Intell. Mechatronics*, 1999, pp. 440–445.



Changhyun Cho received the B.S. and M.S. degrees from Kyunghee University, Seoul, Korea, in 1997 and 1999, respectively, and the Ph.D. degree from Korea University, Seoul, in 2005, all in mechanical engineering.

He joined the Center for Intelligent Robotics, Frontier 21 Program at the Korea Institute of Science and Technology, Seoul, in 2005. His current research interests are mechanism design and control of robotic systems.



Jae-Bok Song received the B.S. and M.S. degrees from Seoul National University, Seoul, Korea, in 1983 and 1985, respectively, and the Ph.D. degree from the Massachusetts Institute of Technology, Cambridge, in 1992, all in mechanical engineering.

He joined the faculty of the Department of Mechanical Engineering, Korea University, Seoul, in 1993, where he has been a Full Professor since 2002. His current research interests are robot navigation, and design and control of robotic systems including haptic devices and field robots.



Munsang Kim received the B.S. and M.S. degrees in mechanical engineering from Seoul National University, Seoul, Korea, in 1980 and 1982, respectively, and the Ph.D. in robotics from the Technical University of Berlin, Berlin, Germany, in 1987.

Since 1987, he has been working as a Research Scientist at the Korea Institute of Science and Technology, Seoul. He has been leading the Advanced Robotics Research Center since 2000 where he became the Director of the "Intelligent Robot—The Frontier 21 Program" in October 2003. His current

research interests are design and control of novel mobile manipulation systems, haptic device design and control, and sensor application to intelligent robots.